A Multi-Task Temporal Fusion Framework for 48 h-Ahead Joint Prediction of Dam Crack Responses and Rebar Stress from Multi-Source Monitoring Data

Binbin Liu *, Mingming Wang , Xiaolei Zhu , Wanbo Zhang

Posted Date: 21 May 2026

doi: 10.20944/preprints202605.1441.v1

Keywords: dam health monitoring; crack prediction; rebar stress; multi-task learning; temporal fusion; monitoring data; buildings

 doi:10.20944/preprints202605.1441.v1

Article

A Multi-Task Temporal Fusion Framework for 48 h-Ahead Joint Prediction of Dam Crack Responses and Rebar Stress from Multi-Source Monitoring Data

Binbin Liu [1,2,*], Mingming Wang [1,2], Xiaolei Zhu [1,2] and Wanbo Zhang [1,2]

[1] Anhui and Huaihe River Institute of Hydraulic Research, Hefei 230088, China
[2] Anhui Key Laboratory of Water Science and Smart Water Conservancy, Hefei 230088, China
* Correspondence: 2627128848@qq.com

Abstract

Crack opening and reinforcement stress are two complementary indicators of the service state of reinforced concrete hydraulic structures, yet they are often predicted separately. This study develops a data-driven multi-task temporal fusion framework for joint 48 h-ahead prediction of dam crack responses and rebar stress using multi-source monitoring data. The measured data comprise five crack-monitoring series, five rebar-stress series, local temperature channels, reservoir water level, antecedent rainfall, and an auxiliary environmental signal from 2021-03-11 to 2025-03-06. Target responses are aligned only at common measured timestamps; no synthetic target observations are introduced. A residual multi-task temporal fusion network (MTTF-Net) is proposed with a shared Transformer encoder, attention pooling, task-specific decoders, and a response-continuity regularization term. The model is compared with persistence, Ridge regression, random forest, Extra Trees, XGBoost, and GRU baselines under a chronological train/validation/test split. On the independent test period, Ridge regression obtains the lowest overall RMSE (2.2968), whereas MTTF-Net provides the lowest crack RMSE (0.0141), the lowest overall MAE (1.0035), and the second-best overall RMSE (2.3813). These results indicate that the monitoring data contain a strong linear autoregressive component, while multi-task temporal fusion improves nonlinear crack-response prediction and remains competitive for stress forecasting. The source code is prepared as a public implementation package, whereas the measured monitoring dataset is subject to data-owner restrictions.

Keywords: dam health monitoring; crack prediction; rebar stress; multi-task learning; temporal fusion; monitoring data; buildings

1. Introduction

Long-term structural health monitoring (SHM) provides the empirical basis for evaluating the service condition of dams, retaining structures, bridges, and reinforced concrete infrastructure. Recent review work on concrete dam monitoring has emphasized the transition from isolated instrument interpretation toward integrated data processing, behaviour modelling, and safety decision support [1]. Deng et al. further organized dam health monitoring studies from data preprocessing to behaviour assessment, showing that long-term monitoring systems increasingly depend on reliable data-driven modelling pipelines [2]. For displacement-based concrete dam SHM, Wang et al. summarized recent observation-data modelling practices and highlighted the importance of environmental actions such as water level, temperature, and rainfall [3]. In the Buildings literature, Deng et al. reviewed bridge SHM as a complete chain of sensing technology, data processing, early warning, and damage identification [4]; Vijayan et al. discussed intelligent technologies and IoT-enabled SHM for civil engineering structures [5]; Wang and Ke reviewed implementation factors for sustainable civil-infrastructure SHM [6]; and Dadras Eslamlou and Huang summarized artificial-neural-network surrogate models for

 doi:10.20944/preprints202605.1441.v1

civil-structure SHM [7]. These studies collectively indicate that modern SHM research is moving toward multi-source sensing, automated data management, and interpretable predictive models.

1.1. Research Status

Dam prediction studies have mainly focused on deformation, displacement, seepage, or stress indicators. Madiniyeti et al. combined sparrow search optimization with LSTM for concrete dam deformation prediction, showing the utility of optimized recurrent networks for monitoring sequences [8]. Zhang et al. proposed a DenseNet-LSTM deformation model with feature selection for concrete gravity dams, which strengthened nonlinear feature extraction before temporal prediction [9]. He and Li used measured prototype temperature data to improve the interpretability of dam deformation forecasting, emphasizing that environmental variables should be treated as physical drivers rather than merely auxiliary inputs [10]. Yin and Wu developed a separate modelling technique for concrete dam deformation, reflecting the long-standing idea that different monitoring components may require different response mechanisms [11]. Wen et al. introduced a combined model based on multiple regression and stacked GRUs for concrete dam deformation prediction [12], while Li et al. proposed DRLSTM as a dual-stage deep-learning model driven by raw dam monitoring data [13]. Wei et al. used a Pearson K-means multi-head attention model for deformation prediction during first impoundment of super-high dams [14]. In Buildings, Wang et al. recently proposed an LSTM sequence-to-sequence model with chaos-based arithmetic optimization and attention for dam deformation prediction, illustrating the journal's interest in dam-oriented intelligent monitoring models [15]. For stress-related dam behaviour, Tao et al. estimated in-service concrete dam stress from deformation data using a hybrid SIE-APSO-CNN-LSTM framework [16]. These studies provide strong methodological references, but most of them predict one response type at a time.

Crack monitoring has developed along a partly separate line. Goszczynska et al. experimentally analysed crack-width development in reinforced concrete beams, providing a mechanics-oriented reference for crack evolution under load [17]. Cramer et al. simulated crack propagation in reinforced concrete elements, showing how crack behaviour can be connected to structural response mechanisms [18]. Ganasan et al. used machine-learning models to predict crack width in reinforced concrete beam-column joints under lateral cyclic loading [19]. Razavi Tosee et al. proposed a hybrid grey-wolf-optimizer neural network for crack-width prediction in CFRP-strengthened RC slabs and published the study in Buildings [20]. Rao et al. developed an attention recurrent residual U-Net for pixel-level concrete crack-width prediction from images [21]. Chen et al. used deep learning for building surface crack detection in Buildings, representing image-based crack inspection rather than time-series monitoring [22]. Laxman et al. combined automated crack detection with crack-depth prediction for reinforced concrete structures using deep learning [23]. These works confirm the importance of crack indicators, but most focus on laboratory members or image data rather than long-term multi-source monitoring series.

Another related stream concerns sensing, data quality, and AI-assisted SHM workflows. Malekloo et al. reviewed machine learning for SHM with attention to emerging high-dimensional data sources [24]. Mishra et al. discussed IoT-based SHM for civil engineering structures, which is relevant to database-oriented monitoring systems [25]. Jayawickrema et al. reviewed fibre-optic sensing and deep learning for civil-structure SHM [26], and Hassani and Dackermann surveyed advanced sensor technologies for nondestructive testing and SHM [27]. Luleci et al. reviewed generative adversarial networks in civil SHM, mainly for data generation, anomaly handling, and data restoration tasks [28]. In Buildings, Nong et al. proposed a multimodal deep-neural-network method for SHM sensor-data anomaly diagnosis, showing that monitoring data quality itself must be modelled carefully [29]; Kordestani et al. developed an output-only energy-based damage detection method using structural acceleration response trends [30]. For trustworthy deployment, Sun et al. reviewed explainable and human-in-the-loop bridge SHM and risk prognosis [31], while Xu et al. discussed few-shot learning for civil-infrastructure structural health diagnosis [32]. These studies motivate a conservative experimental design in which target values are not fabricated and chronological validation is preferred.

 doi:10.20944/preprints202605.1441.v1

The forecasting methodology also benefits from recent general time-series research. Zhou et al. proposed Informer for efficient long-sequence time-series forecasting with Transformer-style attention [33]. Deng et al. developed a multi-view multi-task learning framework for multivariate time-series forecasting, which is conceptually close to joint prediction of multiple structural responses [34]. Song et al. reviewed deep-learning-based time-series forecasting and summarized the development from recurrent networks to attention-based models [35]. Cini et al. reviewed graph deep learning for time-series forecasting, emphasizing relational modelling when multiple sensors interact [36]. These methods suggest that crack and rebar-stress responses should not necessarily be modelled as independent scalar targets when they are driven by shared environmental and structural states.

1.2. Research Gap and Contributions

Despite this progress, a gap remains for joint prediction of dam crack responses and rebar stress from field monitoring data. Crack opening reflects local concrete damage and joint movement, whereas rebar stress reflects internal force redistribution in reinforced components. The two response groups are physically related, but the local monitoring files available in this project do not provide a verified one-to-one mapping between crack sensors and rebar-stress sensors. Imposing artificial pairs would therefore introduce an engineering assumption not supported by the data. In addition, field monitoring data are not laboratory data: sampling frequencies differ, environmental variables may be sampled more frequently than response variables, and target interpolation can create false supervision. A defensible joint model must therefore align measured target timestamps conservatively, use environmental variables only as observed contextual inputs, and compare the proposed model with strong persistence and linear autoregressive baselines.

This study therefore builds a reproducible Buildings-style manuscript package around a joint crack–stress prediction problem. The contributions are as follows:

1. An aligned multi-source monitoring dataset is constructed from measured crack, rebar-stress, temperature, reservoir water-level, rainfall, and auxiliary environmental CSV files. Target responses are not interpolated or synthetically augmented.
2. A residual multi-task temporal fusion network (MTTF-Net) is formulated to predict the crack vector and rebar-stress vector jointly at a 48 h forecast horizon.
3. Seven methods are benchmarked under the same chronological train/validation/test split: persistence, Ridge, random forest, Extra Trees, XGBoost, GRU, and MTTF-Net.
4. Publication-ready figures, equations, symbol definitions, and LaTeX tables are generated directly from the experimental outputs.

2. Materials and Data Construction

2.1. Monitoring Variables

The local monitoring archive contains five crack response files, five rebar-stress files, reservoir water level, rainfall, and auxiliary environmental measurements. Each crack and rebar file has three columns: timestamp, local temperature, and the measured response. The reservoir water level and rainfall files are sampled at a higher frequency than the response files. The raw material is organized in the project directory under `01_data/raw`. The patent document and legacy database access scripts are retained as references but are not used to generate any synthetic observations.

The aligned response period extends from 2021-03-11 07:00:00 to 2025-03-06 07:00:00. All crack and rebar target responses are merged using their common measured timestamps. This inner-join strategy is conservative: it reduces the number of usable records but avoids fabricating target values. Environmental variables are then aligned to the response timestamps by nearest or backward as-of lookup because those variables are sampled more frequently. The final aligned table contains 4281 timestamps and produces 4255 supervised sequences when using a 21-sample historical window and a six-step forecast horizon. With an 8 h response interval, this corresponds to approximately 7 days of input history and 48 h ahead prediction.

 doi:10.20944/preprints202605.1441.v1

Table 1. Dataset construction settings.

Item	Value
Aligned timestamps	4281
Supervised sequences	4255
Input features	29
Prediction targets	10
Input window L	21 samples (approximately 7 days)
Forecast horizon H	6 samples (approximately 48 h)

Table 2. Monitoring response variables used in the aligned joint-prediction dataset.

Group	Sensor	Raw records	Aligned records	Start	End
crack	J01-01	4367	4281	2021-03-11	2025-03-06
crack	J02-05	4367	4281	2021-03-11	2025-03-06
crack	J10-01	4343	4281	2021-03-11	2025-03-06
crack	J13-01	4345	4281	2021-03-11	2025-03-06
crack	J15-07	4342	4281	2021-03-11	2025-03-06
rebar_stress	R02-02	4367	4281	2021-03-11	2025-03-06
rebar_stress	R02-03	4364	4281	2021-03-11	2025-03-06
rebar_stress	R03-01	4364	4281	2021-03-11	2025-03-06
rebar_stress	R03-02	4364	4281	2021-03-11	2025-03-06
rebar_stress	R15-01	4342	4281	2021-03-11	2025-03-06

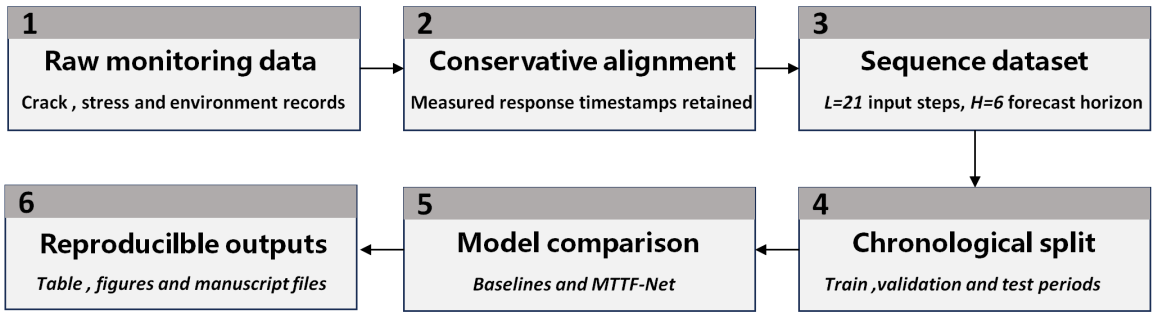

Figure 1. Workflow used to construct the joint-prediction dataset, train benchmark models, and generate the manuscript material.

The public implementation package for MTTF-Net is available at https://github.com/ArthurCode-prod/MTFF-Net. The repository provides the reusable model, data-reading interfaces, training and evaluation scripts, and a toy smoke-test example; the measured monitoring dataset used for the reported experiments is not included in the public repository.

 doi:10.20944/preprints202605.1441.v1

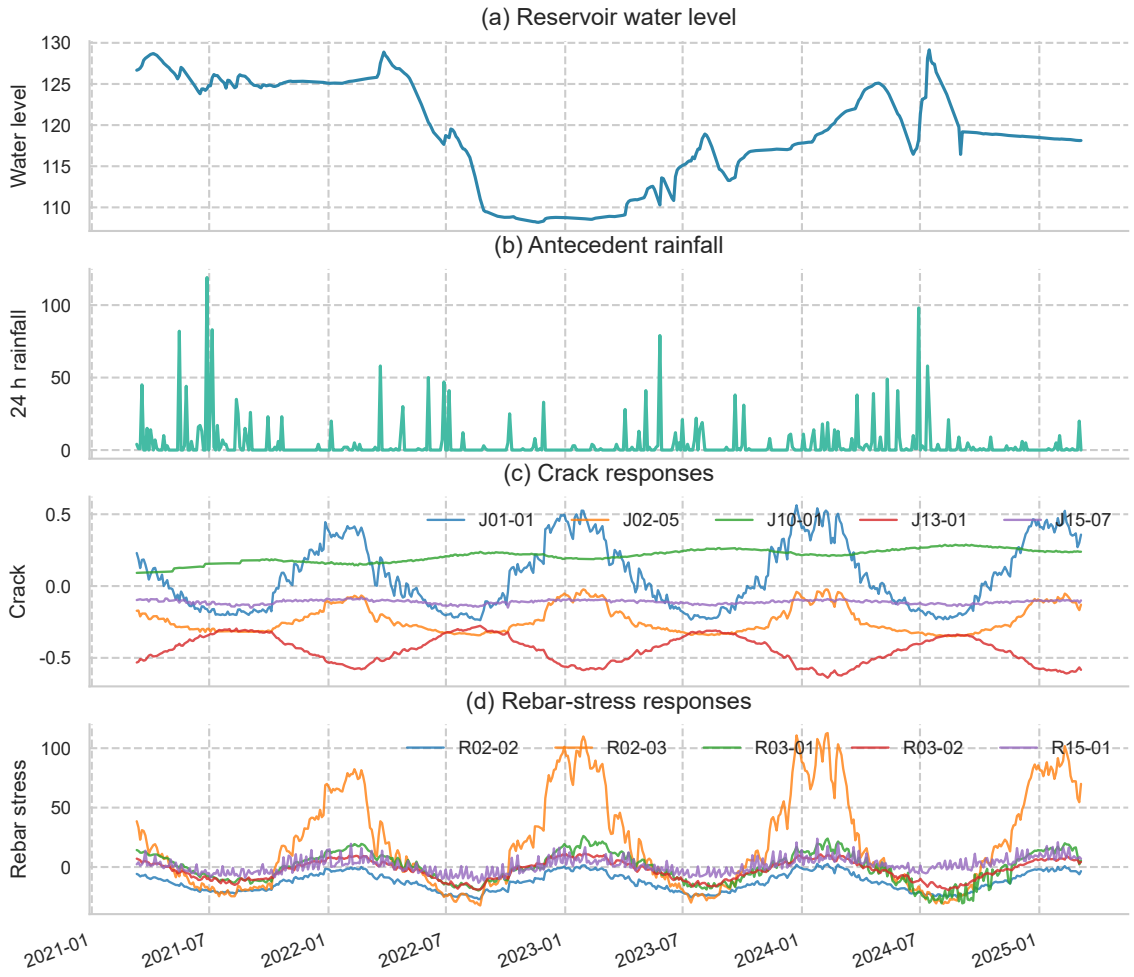

Figure 2. Overview of representative aligned monitoring variables: reservoir water level, antecedent rainfall, crack responses, and rebar-stress responses. The plotted series are down-sampled only for visualization.

 doi:10.20944/preprints202605.1441.v1

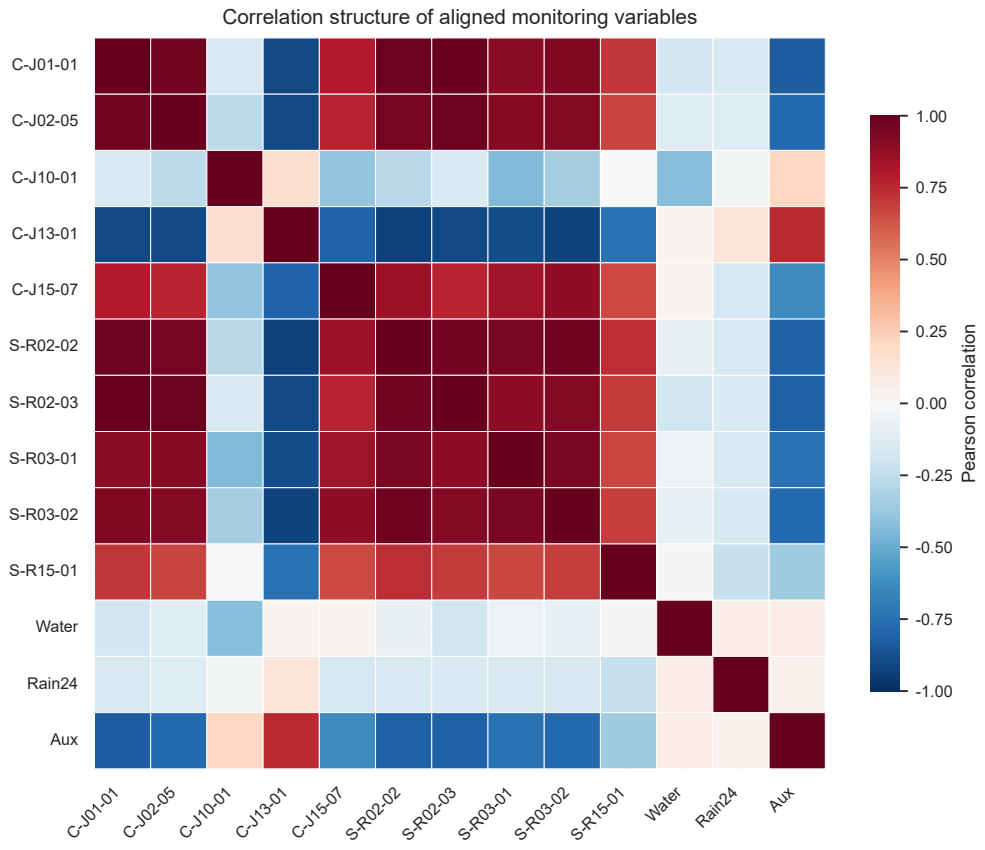

Figure 3. Pearson correlation matrix of aligned target and environmental variables. The matrix is used for exploratory interpretation only and is not used to remove or create target observations.

3. Mathematical Formulation

Let t denote the index of an aligned response timestamp. The crack response vector and rebar-stress response vector are denoted by

$$\mathbf{c}_t = \left[c_{t,1}, c_{t,2}, \ldots, c_{t,Q_c}\right]^\top, \qquad \mathbf{s}_t = \left[s_{t,1}, s_{t,2}, \ldots, s_{t,Q_s}\right]^\top, \tag{1}$$

where $Q_c = 5$ and $Q_s = 5$ in this study. The stacked response vector is

$$\mathbf{r}_t = \begin{bmatrix} \mathbf{c}_t \\ \mathbf{s}_t \end{bmatrix} \in \mathbb{R}^{Q_c+Q_s}. \tag{2}$$

At timestamp t, the input feature vector $\mathbf{x}_t \in \mathbb{R}^P$ contains historical crack and rebar responses, local temperatures, reservoir water level, antecedent rainfall features, the auxiliary environmental signal, and calendar encodings. For a look-back window of length L, the input matrix is

$$\mathbf{X}_{t-L+1:t} = \begin{bmatrix} \mathbf{x}_{t-L+1}^\top \\ \mathbf{x}_{t-L+2}^\top \\ \vdots \\ \mathbf{x}_t^\top \end{bmatrix} \in \mathbb{R}^{L\times P}. \tag{3}$$

The supervised learning set is defined as

$$\mathcal{D} = \left\{\left(\mathbf{X}_{t-L+1:t}, \mathbf{c}_{t+H}, \mathbf{s}_{t+H}\right)\right\}_{t=L}^{T-H}, \tag{4}$$

 doi:10.20944/preprints202605.1441.v1

where $H = 6$ is the forecast horizon. For any scalar variable z, standardization is performed using parameters estimated from the training split only:

$$\widetilde{z} = \frac{z - \mu_z}{\sigma_z + \epsilon}, \tag{5}$$

where μ_z is the training-set mean, σ_z is the training-set standard deviation, and ϵ is a small numerical constant.

Table 3. Main mathematical symbols used in the proposed formulation.

Symbol	Definition	Unit/range
t	Response timestamp index	dimensionless
L	Length of the historical input window	samples
H	Forecast horizon	samples
P	Number of input features	dimensionless
Q_c	Number of crack targets	dimensionless
Q_s	Number of rebar-stress targets	dimensionless
$\mathbf{x}_t$	Input feature vector at timestamp t	$\mathbb{R}^P$
$\mathbf{X}_{t-L+1:t}$	Historical input matrix ending at timestamp t	$\mathbb{R}^{L\times P}$
$\mathbf{c}_{t+H}$	Crack response vector to be forecast	$\mathbb{R}^{Q_c}$
$\mathbf{s}_{t+H}$	Rebar-stress response vector to be forecast	$\mathbb{R}^{Q_s}$
$\widehat{\mathbf{c}}_{t+H}$	Predicted crack vector	$\mathbb{R}^{Q_c}$
$\widehat{\mathbf{s}}_{t+H}$	Predicted rebar-stress vector	$\mathbb{R}^{Q_s}$
$\mathbf{h}_t$	Shared latent representation from MTTF-Net	$\mathbb{R}^d$
Θ	Trainable model parameters	–
$\mathcal{L}$	Joint training loss	–

4. Proposed MTTF-Net

4.1. Shared Temporal Encoder

MTTF-Net uses a shared temporal encoder for both target groups. The standardized input matrix is projected into a d-dimensional latent space:

$$\mathbf{Z}_t^{(0)} = \widetilde{\mathbf{X}}_{t-L+1:t}\mathbf{W}_e + \mathbf{E}_{\text{pos}}, \tag{6}$$

where $\mathbf{W}_e \in \mathbb{R}^{P\times d}$ is the input projection matrix and $\mathbf{E}_{\text{pos}} \in \mathbb{R}^{L\times d}$ is the learnable positional embedding.

For a Transformer encoder layer, multi-head attention is computed as

$$\text{MHA}(\mathbf{Q},\mathbf{K},\mathbf{V}) = \text{Concat}(\mathbf{O}_1,\ldots,\mathbf{O}_M)\mathbf{W}^O, \tag{7}$$

with

$$\mathbf{O}_m = \text{softmax}\left(\frac{\mathbf{Q}\mathbf{W}_m^Q(\mathbf{K}\mathbf{W}_m^K)^\top}{\sqrt{d_k}}\right)\mathbf{V}\mathbf{W}_m^V, \tag{8}$$

where M is the number of attention heads, d_k is the key dimension, and $\mathbf{W}_m^Q$, $\mathbf{W}_m^K$, $\mathbf{W}_m^V$, and $\mathbf{W}^O$ are trainable matrices. A lightweight one-dimensional convolutional residual block is applied after the

 doi:10.20944/preprints202605.1441.v1

Transformer encoder to enhance local temporal variation. Attention pooling then maps the encoded sequence to a shared state:

$$\alpha_\ell = \frac{\exp\left(\mathbf{u}^\top \tanh(\mathbf{W}_a \mathbf{z}_{t,\ell} + \mathbf{b}_a)\right)}{\sum_{j=1}^{L} \exp\left(\mathbf{u}^\top \tanh\left(\mathbf{W}_a \mathbf{z}_{t,j} + \mathbf{b}_a\right)\right)}, \qquad \mathbf{h}_t = \sum_{\ell=1}^{L} \alpha_\ell \mathbf{z}_{t,\ell}, \tag{9}$$

where $\mathbf{z}_{t,\ell}$ is the encoded latent vector at the ℓth position in the input window.

4.2. Residual Multi-Task Decoders

Because the monitoring responses are highly continuous over time, MTTF-Net predicts response increments relative to the last observed standardized response. The standardized prediction is

$$\begin{bmatrix} \widehat{\widetilde{\mathbf{c}}}_{t+H} \\ \widehat{\widetilde{\mathbf{s}}}_{t+H} \end{bmatrix} = \begin{bmatrix} \widetilde{\mathbf{c}}_t \\ \widetilde{\mathbf{s}}_t \end{bmatrix} + \begin{bmatrix} g_c(\mathbf{h}_t; \Theta_c) \\ g_s(\mathbf{h}_t; \Theta_s) \end{bmatrix}, \tag{10}$$

where $g_c(\cdot)$ and $g_s(\cdot)$ are task-specific fully connected decoders for crack and stress responses. All trainable weights and biases in the embedding, encoder, pooling module, and two decoders are collectively denoted by Θ.

The loss function combines target errors and a weak continuity regularization term:

$$\mathcal{L}(\Theta) = \frac{\lambda_c}{NQ_c} \sum_{i=1}^{N} \left\| \widehat{\widetilde{\mathbf{c}}}_i - \widetilde{\mathbf{c}}_i \right\|_2^2 + \frac{\lambda_s}{NQ_s} \sum_{i=1}^{N} \left\| \widehat{\widetilde{\mathbf{s}}}_i - \widetilde{\mathbf{s}}_i \right\|_2^2 + \frac{\lambda_\Delta}{N(Q_c+Q_s)} \sum_{i=1}^{N} \left\| \widehat{\widetilde{\mathbf{r}}}_i - \widetilde{\mathbf{r}}_{i,0} \right\|_2^2 + \lambda_\Theta \|\Theta\|_2^2. \tag{11}$$

Here, N is the number of training sequences, $\widetilde{\mathbf{r}}_{i,0}$ is the last observed standardized stacked response in the input window, λ_c and λ_s balance the two task groups, λ_Δ controls response-continuity regularization, and λ_Θ denotes weight decay.

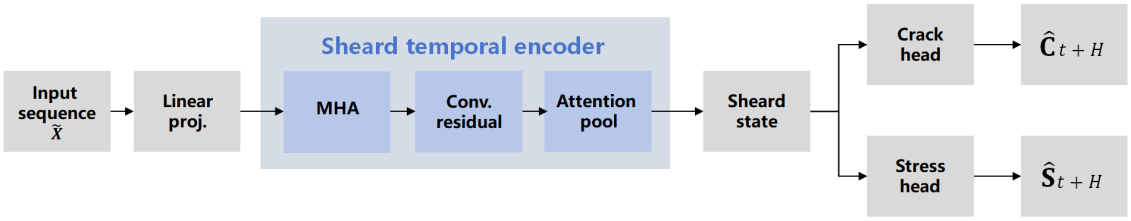

Figure 4. Architecture of MTTF-Net. A shared temporal encoder processes the multi-source sequence, and two task-specific residual heads predict the 48 h-ahead crack and rebar-stress vectors. MHA denotes multi-head attention.

5. Experimental Design

5.1. Benchmark Algorithms

The proposed model is compared with six baselines. Persistence uses the last observed target vector as the forecast. Ridge regression represents a strong linear autoregressive benchmark. Random forest and Extra Trees represent bagged tree ensembles. XGBoost represents boosted tree learning. A GRU network represents a recurrent deep-learning baseline. These models cover naive persistence, linear regression, ensemble learning, boosted nonlinear regression, recurrent neural forecasting, and the proposed attention-based multi-task temporal fusion.

All methods use the same input window, target horizon, feature matrix, and target vector. The chronological split contains 2978 training sequences, 638 validation sequences, and 639 test sequences. Standardization is fitted only on the training split. Tree and Ridge models are trained on the combined training and validation data after hyperparameters are fixed. Neural models use the validation split for early stopping.

 doi:10.20944/preprints202605.1441.v1

5.2. Metrics

For a target group with K scalar observations in the test set, the mean absolute error, root mean squared error, and coefficient of determination are

$$\mathrm{MAE} = \frac{1}{K}\sum_{k=1}^{K}|y_k - \widehat{y}_k|, \tag{12}$$

$$\mathrm{RMSE} = \sqrt{\frac{1}{K}\sum_{k=1}^{K}(y_k - \widehat{y}_k)^2}, \tag{13}$$

$$R^2 = 1 - \frac{\sum_{k=1}^{K}(y_k - \widehat{y}_k)^2}{\sum_{k=1}^{K}(y_k - \bar{y})^2}, \qquad \bar{y} = \frac{1}{K}\sum_{k=1}^{K} y_k. \tag{14}$$

Metrics are reported for all targets together and separately for crack and rebar-stress groups.

6. Results

6.1. Overall Prediction Accuracy

The benchmark results show that the 48 h-ahead task remains strongly autoregressive. Ridge regression has the lowest overall RMSE (2.2968) and stress RMSE (3.2481). However, MTTF-Net has the lowest overall MAE (1.0035) and the lowest crack RMSE (0.0141), indicating that the nonlinear shared temporal encoder is particularly useful for the crack-response group. Compared with persistence, MTTF-Net reduces the overall RMSE from 2.6590 to 2.3813, corresponding to a 10.44% reduction, and improves the overall R^2 from 0.9796 to 0.9837. Random forest, Extra Trees, and GRU are less competitive on this dataset, which suggests that simple nonlinear model capacity is not sufficient when the response is dominated by linear temporal inertia.

Table 4. Test-set performance for 48 h-ahead joint prediction. The chronological test set was not used in model fitting or early stopping.

Model	MAE	RMSE	R^2	Crack RMSE	Stress RMSE
Persistence	1.1393	2.6590	0.9796	0.0164	3.7604
Ridge	1.0683	2.2968	0.9848	0.0149	3.2481
Random Forest	1.5439	3.3355	0.9680	0.0269	4.7170
Extra Trees	1.4552	3.0957	0.9724	0.0239	4.3780
XGBoost	1.1011	2.3957	0.9835	0.0144	3.3880
GRU	1.3949	2.9686	0.9746	0.0196	4.1982
MTTF-Net	1.0035	2.3813	0.9837	0.0141	3.3676

 doi:10.20944/preprints202605.1441.v1

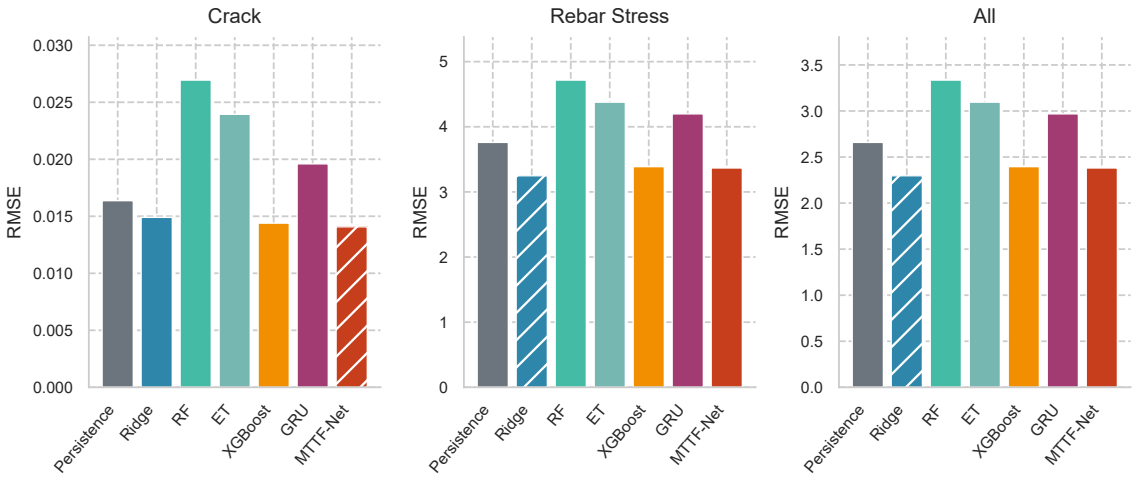

Figure 5. RMSE comparison for crack targets, rebar-stress targets, and all targets. Hatched bars indicate the best model in each panel.

6.2. Per-Target Performance of MTTF-Net

The per-target results in Table 5 show that MTTF-Net maintains high R^2 values for most response channels, while the R15-01 stress channel is more difficult during the test period. The model is especially accurate for crack channels because their amplitudes are smaller and their temporal evolution is smoother in the test period. Stress channels have larger numerical ranges and more abrupt local variations, which explains their higher absolute RMSE.

Table 5. Per-target test performance of MTTF-Net for the 48 h-ahead prediction task.

Target	Group	MAE	RMSE	R^2
crack_J01-01	crack	0.0211	0.0296	0.9860
crack_J02-05	crack	0.0061	0.0083	0.9935
crack_J10-01	crack	0.0025	0.0031	0.9703
crack_J13-01	crack	0.0035	0.0045	0.9979
crack_J15-07	crack	0.0029	0.0037	0.9081
rebar_R02-02	rebar_stress	0.6450	0.8378	0.9902
rebar_R02-03	rebar_stress	3.1063	4.2088	0.9906
rebar_R03-01	rebar_stress	3.2830	5.1404	0.8950
rebar_R03-02	rebar_stress	0.5122	0.6609	0.9946
rebar_R15-01	rebar_stress	2.4528	3.3806	0.6192

 doi:10.20944/preprints202605.1441.v1

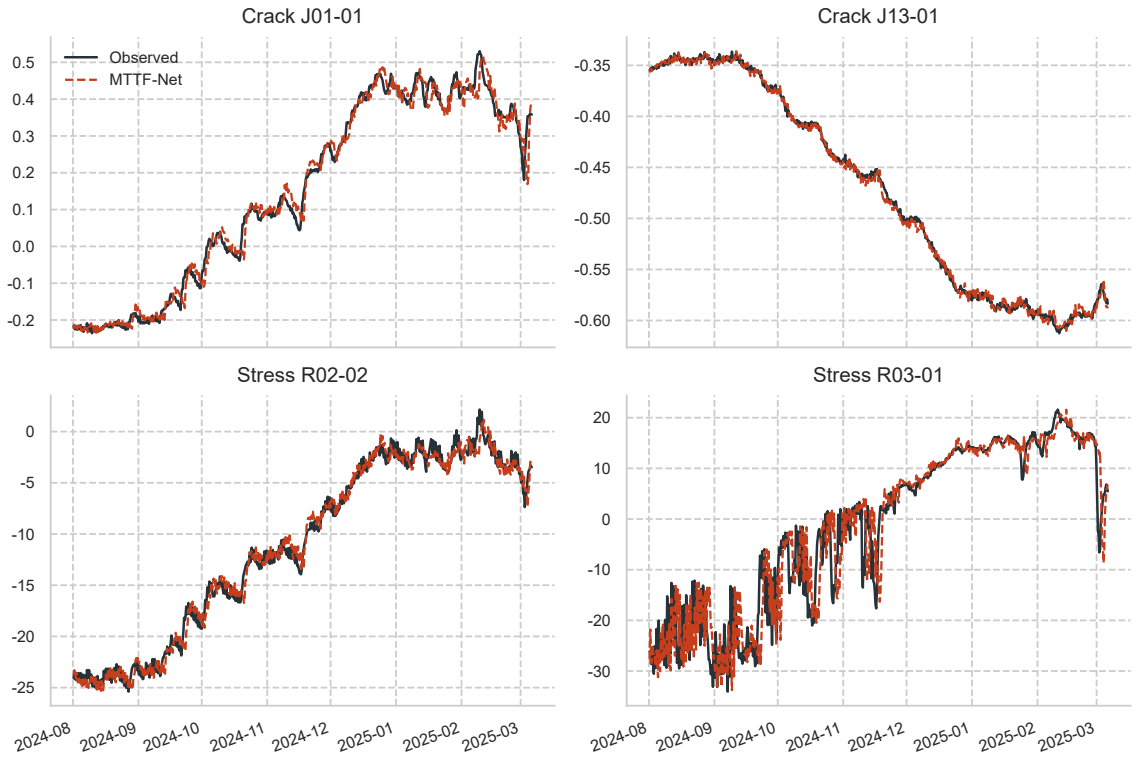

Figure 6. Observed and predicted test-period time series for representative crack and rebar-stress targets using MTTF-Net.

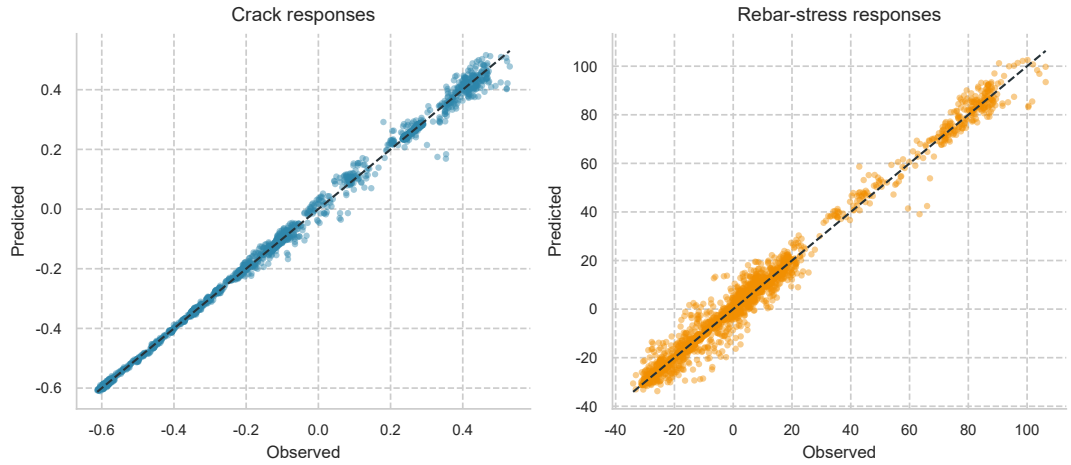

Figure 7. Observed-versus-predicted scatter plots for the MTTF-Net test predictions. The dashed line is the ideal one-to-one line.

6.3. Feature Relevance

Random-forest feature importance is used only as an auxiliary exploratory tool. It is not used to select the final model inputs. Figure 8 shows that historical response channels dominate the benchmark feature ranking, while water level, rainfall accumulation, and temperature channels provide contextual information. This is consistent with the strong performance of persistence and Ridge regression and confirms that any nonlinear model must first respect the response-continuity structure of the monitoring data.

 doi:10.20944/preprints202605.1441.v1

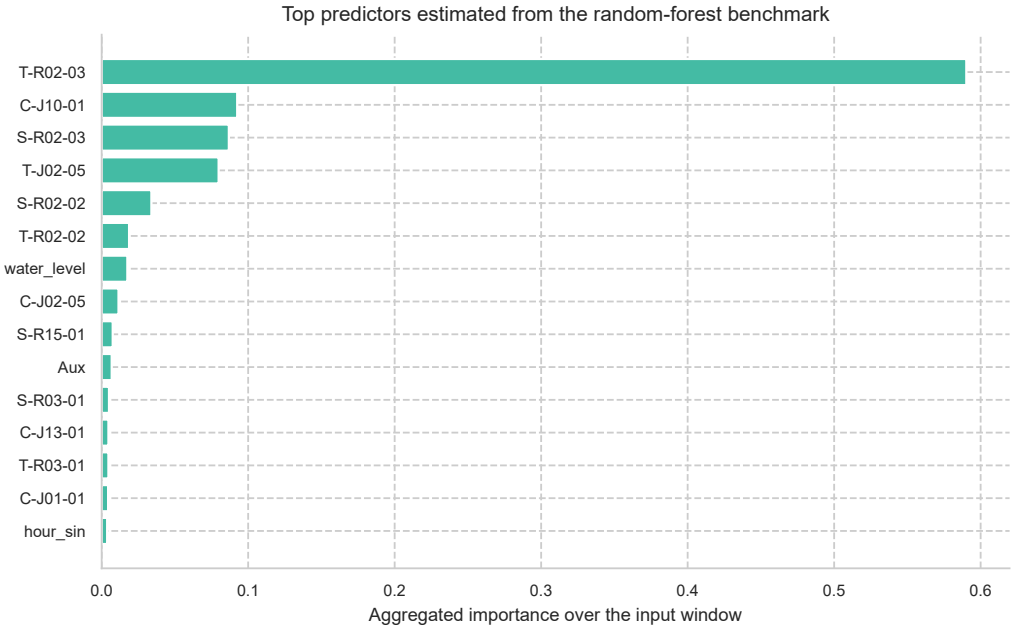

Figure 8. Top 15 predictors ranked by the random-forest benchmark after aggregating feature importance over the input window.

6.4. Computational Cost

The experiments were executed on the local workstation CPU. MTTF-Net required early-stopped neural training but remained tractable for the dataset size. The computational burden is acceptable for offline model development and periodic retraining; for real-time warning deployment, inference cost is negligible compared with data acquisition and database access.

Table 6. Wall-clock training and inference time measured on the local workstation.

Model	Time (s)	Epochs
Persistence	0.00	–
Ridge	0.02	–
Random Forest	76.21	–
Extra Trees	34.92	–
XGBoost	28.76	–
GRU	57.85	61
MTTF-Net	46.21	27

7. Discussion

7.1. Why Ridge Is a Strong Baseline

The results demonstrate that the dataset has a strong linear autoregressive component. This is reasonable for dam monitoring: crack and stress responses usually vary continuously under slowly changing thermal and hydraulic actions. Therefore, a high-capacity nonlinear model is not automatically superior. This finding is important because some recent SHM studies emphasize deep learning without comparing sufficiently strong persistence and linear baselines. In the present study, Ridge regression is not treated as a weak reference but as a serious benchmark.

7.2. Value of Joint Multi-Task Fusion

Although Ridge has the lowest overall RMSE, MTTF-Net provides the best crack RMSE and the best overall MAE. This suggests that joint nonlinear temporal fusion can better track some local crack-response deviations, while stress prediction remains more sensitive to the large-amplitude and abrupt components of rebar measurements. From an engineering perspective, the proposed framework

 doi:10.20944/preprints202605.1441.v1

is useful because it provides a unified crack–stress prediction interface and can be extended with more monitoring channels, physical constraints, or probabilistic warning intervals.

7.3. Limitations

Three limitations should be noted before journal submission. First, the local files do not contain a verified engineering mapping between individual crack sensors and individual rebar-stress sensors. Therefore, this study models all available crack and rebar responses as a joint multi-output vector rather than imposing arbitrary one-to-one sensor pairs. Second, the present results are based on one monitored structure and one chronological test period. External validation on another dam or another construction stage would strengthen the generality of the conclusions. Third, the current model produces deterministic point forecasts. For operational warning, probabilistic intervals, split conformal prediction, or Bayesian uncertainty quantification would be valuable extensions.

8. Conclusions

This study constructed a reproducible manuscript package for joint 48 h-ahead prediction of dam crack responses and rebar stress from measured multi-source monitoring data. The aligned dataset contains 4281 common response timestamps and 4255 supervised sequences from five crack targets and five rebar-stress targets. No synthetic target responses were created.

The proposed MTTF-Net uses a shared Transformer encoder, attention pooling, response-residual decoding, and multi-task loss. In the chronological test period, Ridge regression achieved the lowest overall RMSE of 2.2968, while MTTF-Net achieved the lowest crack RMSE of 0.0141, the lowest overall MAE of 1.0035, and the second-best overall RMSE of 2.3813. Compared with persistence, MTTF-Net reduced overall RMSE by 10.44%. The findings indicate that the monitored structure exhibits strong linear temporal inertia, but nonlinear multi-task temporal fusion improves crack-response forecasting and offers a flexible framework for integrated crack–stress warning.

Future work should verify sensor correspondence using project metadata, connect the rebuilt code directly to the Kingbase database with secure credentials, extend the model to probabilistic warning intervals, and test transferability across additional structures or monitoring periods.

Author Contributions: Conceptualization, B.L. and M.W.; methodology, B.L.; software, B.L.; validation, B.L. and X.Z.; formal analysis, B.L. and W.Z.; investigation, M.W. and X.Z.; resources, B.L. and M.W.; data curation, W.Z.; writing—original draft preparation, B.L.; writing—review and editing, M.W., X.Z. and W.Z.; visualization, B.L.; supervision, B.L. All authors have read and agreed to the published version of the manuscript.

Funding: This research was funded by the Youth Science and Technology Innovation Program of Anhui and Huaihe River Institute of Hydraulic Research, grant number KY202503.

Institutional Review Board Statement: Not applicable.

Informed Consent Statement: Not applicable.

Data Availability Statement: The open-source implementation is available at https://github.com/ArthurCode-prod/MTFF-Net. The measured monitoring dataset used in this study is not publicly released at this stage because of project confidentiality and data-owner restrictions. The local manuscript workspace contains the processed dataset, generated figures, and tables required for internal reproducibility.

Conflicts of Interest: The authors declare no conflict of interest.

References

1. Prakash, G.; Dugalam, R.; Barbosh, M.; Sadhu, A. Recent advancement of concrete dam health monitoring technology: A systematic literature review. *Structures* **2022**, *44*, 766–784. https://doi.org/10.1016/j.istruc.2022.08.021.
2. Deng, Z.; Gao, Q.; Huang, M.; Wan, N.; Zhang, J.; He, Z. From data processing to behavior monitoring: A comprehensive overview of dam health monitoring technology. *Structures* **2025**, *71*, 108094. https://doi.org/10.1016/j.istruc.2024.108094.

 doi:10.20944/preprints202605.1441.v1

3. Wang, S.; Gu, C.; Liu, Y.; Gu, H.; Xu, B.; Wu, B. Displacement observation data-based structural health monitoring of concrete dams: A state-of-art review. *Structures* **2024**, *68*, 107072. https://doi.org/10.1016/j.istruc.2024.107072.
4. Deng, Z.; Huang, M.; Wan, N.; Zhang, J. The Current Development of Structural Health Monitoring for Bridges: A Review. *Buildings* **2023**, *13*, 1360. https://doi.org/10.3390/buildings13061360.
5. Vijayan, D.S.; Sivasuriyan, A.; Devarajan, P.; Krejsa, M.; Chalecki, M.; Zoltowski, M.; Kozarzewska, A.; Koda, E. Development of Intelligent Technologies in SHM on the Innovative Diagnosis in Civil Engineering-A Comprehensive Review. *Buildings* **2023**, *13*, 1903. https://doi.org/10.3390/buildings13081903.
6. Wang, G.; Ke, J. Literature Review on the Structural Health Monitoring (SHM) of Sustainable Civil Infrastructure: An Analysis of Influencing Factors in the Implementation. *Buildings* **2024**, *14*, 402. https://doi.org/10.3390/buildings14020402.
7. Dadras Eslamlou, A.; Huang, S. Artificial-Neural-Network-Based Surrogate Models for Structural Health Monitoring of Civil Structures: A Literature Review. *Buildings* **2022**, *12*, 2067. https://doi.org/10.3390/buildings12122067.
8. Madiniyeti, J.; Chao, Y.; Li, T.; Qi, H.; Wang, F. Concrete Dam Deformation Prediction Model Research Based on SSA–LSTM. *Applied Sciences* **2023**, *13*, 7375. https://doi.org/10.3390/app13137375.
9. Zhang, Y.; Zhong, W.; Li, Y.; Wen, L. A deep learning prediction model of DenseNet-LSTM for concrete gravity dam deformation based on feature selection. *Engineering Structures* **2023**, *295*, 116827. https://doi.org/10.1016/j.engstruct.2023.116827.
10. He, P.; Li, Y. A Data-Driven Dam Deformation Forecasting and Interpretation Method Using the Measured Prototypical Temperature Data. *Water* **2022**, *14*, 2538. https://doi.org/10.3390/w14162538.
11. Yin, C.; Wu, Z. Separate modeling technique for deformation monitoring of concrete dams. *Structural Health Monitoring* **2022**, *21*, 2968–2989. https://doi.org/10.1177/14759217221079013.
12. Wen, Z.; Zhou, R.; Su, H. MR and stacked GRUs neural network combined model and its application for deformation prediction of concrete dam. *Expert Systems with Applications* **2022**, *201*, 117272. https://doi.org/10.1016/j.eswa.2022.117272.
13. Li, M.; Li, M.; Ren, Q.; Li, H.; Song, L. DRLSTM: A dual-stage deep learning approach driven by raw monitoring data for dam displacement prediction. *Advanced Engineering Informatics* **2022**, *51*, 101510. https://doi.org/10.1016/j.aei.2021.101510.
14. Wei, Y.; Liu, C.; Duan, H.; Wang, Y.; Hu, Y.; Zhu, X.; Tan, Y.; Pei, L. Pearson K-Mean Multi-Head Attention Model for Deformation Prediction of Super-High Dams in First Impoundments. *Water* **2023**, *15*, 1734. https://doi.org/10.3390/w15091734.
15. Wang, L.; Wang, J.; Tong, D.; Wang, X. A Novel Long Short-Term Memory Seq2Seq Model with Chaos-Based Optimization and Attention Mechanism for Enhanced Dam Deformation Prediction. *Buildings* **2024**, *14*, 3675. https://doi.org/10.3390/buildings14113675.
16. Tao, L.; Zheng, D.; Wu, X.; Chen, X.; Liu, Y.; Chen, Z.; Jiang, H. Stress Estimation of Concrete Dams in Service Based on Deformation Data Using SIE–APSO–CNN–LSTM. *Water* **2022**, *15*, 59. https://doi.org/10.3390/w15010059.
17. Goszczyńska, B.; Trąmpczyński, W.; Tworzewska, J. Analysis of Crack Width Development in Reinforced Concrete Beams. *Materials* **2021**, *14*, 3043. https://doi.org/10.3390/ma14113043.
18. Cramer, J.; Javidmehr, S.; Empelmann, M. Simulation of Crack Propagation in Reinforced Concrete Elements. *Applied Sciences* **2021**, *11*, 785. https://doi.org/10.3390/app11020785.
19. Ganasan, R.; Tan, C.G.; Ibrahim, Z.; Nazri, F.M.; Sherif, M.M.; El-Shafie, A. Development of Crack Width Prediction Models for RC Beam-Column Joint Subjected to Lateral Cyclic Loading Using Machine Learning. *Applied Sciences* **2021**, *11*, 7700. https://doi.org/10.3390/app11167700.
20. Razavi Tosee, S.; Faridmehr, I.; Nehdi, M.; Plevris, V.; Valerievich, K. Predicting Crack Width in CFRP-Strengthened RC One-Way Slabs Using Hybrid Grey Wolf Optimizer Neural Network Model. *Buildings* **2022**, *12*, 1870. https://doi.org/10.3390/buildings12111870.
21. Rao, A.S.; Nguyen, T.; Le, S.T.; Palaniswami, M.; Ngo, T. Attention recurrent residual U-Net for predicting pixel-level crack widths in concrete surfaces. *Structural Health Monitoring* **2022**, *21*, 2732–2749. https://doi.org/10.1177/14759217211068859.
22. Chen, Y.; Zhu, Z.; Lin, Z.; Zhou, Y. Building Surface Crack Detection Using Deep Learning Technology. *Buildings* **2023**, *13*, 1814. https://doi.org/10.3390/buildings13071814.

 doi:10.20944/preprints202605.1441.v1

23. Laxman, K.C.; Tabassum, N.; Ai, L.; Cole, C.; Ziehl, P. Automated crack detection and crack depth prediction for reinforced concrete structures using deep learning. *Construction and Building Materials* **2023**, *370*, 130709. https://doi.org/10.1016/j.conbuildmat.2023.130709.
24. Malekloo, A.; Ozer, E.; AlHamaydeh, M.; Girolami, M. Machine learning and structural health monitoring overview with emerging technology and high-dimensional data source highlights. *Structural Health Monitoring* **2022**, *21*, 1906–1955. https://doi.org/10.1177/14759217211036880.
25. Mishra, M.; Lourenço, P.B.; Ramana, G. Structural health monitoring of civil engineering structures by using the internet of things: A review. *Journal of Building Engineering* **2022**, *48*, 103954. https://doi.org/10.1016/j.jobe.2021.103954.
26. Jayawickrema, U.; Herath, H.; Hettiarachchi, N.; Sooriyaarachchi, H.; Epaarachchi, J. Fibre-optic sensor and deep learning-based structural health monitoring systems for civil structures: A review. *Measurement* **2022**, *199*, 111543. https://doi.org/10.1016/j.measurement.2022.111543.
27. Hassani, S.; Dackermann, U. A Systematic Review of Advanced Sensor Technologies for Non-Destructive Testing and Structural Health Monitoring. *Sensors* **2023**, *23*, 2204. https://doi.org/10.3390/s23042204.
28. Luleci, F.; Catbas, F.N.; Avci, O. A literature review: Generative adversarial networks for civil structural health monitoring. *Frontiers in Built Environment* **2022**, *8*. https://doi.org/10.3389/fbuil.2022.1027379.
29. Nong, X.; Luo, X.; Lin, S.; Ruan, Y.; Ye, X. Multimodal Deep Neural Network-Based Sensor Data Anomaly Diagnosis Method for Structural Health Monitoring. *Buildings* **2023**, *13*, 1976. https://doi.org/10.3390/buildings13081976.
30. Kordestani, H.; Zhang, C.; Arab, A. An Output-Only, Energy-Based, Damage Detection Method Using the Trend Lines of the Structural Acceleration Response. *Buildings* **2023**, *13*, 3007. https://doi.org/10.3390/buildings13123007.
31. Sun, Z.; Chen, T.; Meng, X.; Bao, Y.; Hu, L.; Zhao, R. A Critical Review for Trustworthy and Explainable Structural Health Monitoring and Risk Prognosis of Bridges with Human-In-The-Loop. *Sustainability* **2023**, *15*, 6389. https://doi.org/10.3390/su15086389.
32. XU, Y.; FAN, Y.; BAO, Y.; LI, H. Few-shot learning for structural health diagnosis of civil infrastructure. *Advanced Engineering Informatics* **2024**, *62*, 102650. https://doi.org/10.1016/j.aei.2024.102650.
33. Zhou, H.; Zhang, S.; Peng, J.; Zhang, S.; Li, J.; Xiong, H.; Zhang, W. Informer: Beyond Efficient Transformer for Long Sequence Time-Series Forecasting. *Proceedings of the AAAI Conference on Artificial Intelligence* **2021**, *35*, 11106–11115. https://doi.org/10.1609/aaai.v35i12.17325.
34. Deng, J.; Chen, X.; Jiang, R.; Song, X.; Tsang, I.W. A Multi-View Multi-Task Learning Framework for Multi-Variate Time Series Forecasting. *IEEE Transactions on Knowledge and Data Engineering* **2022**, pp. 1–16. https://doi.org/10.1109/TKDE.2022.3218803.
35. Song, X.; Deng, L.; Wang, H.; Zhang, Y.; He, Y.; Cao, W. Deep learning-based time series forecasting. *Artificial Intelligence Review* **2024**, *58*. https://doi.org/10.1007/s10462-024-10989-8.
36. Cini, A.; Marisca, I.; Zambon, D.; Alippi, C. Graph Deep Learning for Time Series Forecasting. *ACM Computing Surveys* **2025**, *57*, 1–34. https://doi.org/10.1145/3742784.